Acta Polytechnica CTU Proceedings **9**:26–31, 2017
doi:10.14311/APP.2017.9.0026

available online at http://ojs.cvut.cz/ojs/index.php/app

REMOVAL OF DIQUATERNARY AMMONIUM CATIONS FROM AS-SYNTHESIZED SSZ-16 ZEOLITE

Tatana Supinkova[a, c, *], Ivan Jirka[a], Jan Drahokoupil[b, d], Jan Langmaier[a], Vlastimil Fila[c], Libor Brabec[a], Milan Kocirik[a]

[a] *J. Heyrovsky Institute of Physical Chemistry,Czech Academy of Sciences, Dolejskova 2155/3, Prague 8, Czech Republic*

[b] *Faculty of Nuclear Sciences and Physical Engineering, Czech Technical University, Trojanova 13, Prague 2, Czech Republic*

[c] *Faculty of Inorganic Technologies, University of Chemistry and Technology in Prague, Technicka 5, Prague 6, Czech Republic*

[d] *Institute of Physics, Czech Academy of Sciences, Na Slovance 1999/2, Prague 8, Czech Republic*

[*] corresponding author: tatana.supinkova@jh-inst.cas.cz

Abstract. Zeolites are stable microporous aluminosilicates with numerous applications in chemical technology such as separation of species and catalytic transformations. Our study is focused on a weakly explored zeolite SSZ-16 with pore constrictions defined by 8-membered oxygen rings. Key results are the preparation of Et_6-diquat-5 dication used as a structure directing agent (SDA) and finding the optimum synthesis conditions with respect to zeolite phase purity. Stability of SDA was examined in conditions similar to those of autoclave synthesis (concentration, pH, temperature). Moreover, the content and location of SDA species in zeolite phase and conditions of SDA decomposition were investigated.

Keywords: Zeolite, Hydrothermal Synthesis, SSZ-16, AFX, Et_6-diquat-5^{2+}.

1. Introduction

Zeolites and zeolite-like materials consist of tetraedral building units TO_4 where T are central atoms most frequently Si and Al^+. Tetraedra are linked to each other through oxygen atoms. The spaceous arrangement of tetrahedra form as a rule microporous structure where micropores take the shape of regular voids (channels and/or cavities) which are repeated through the crystals with the regularity of the crystalline structure. In zeolites, T-atoms can be replaced by isomorphous substitution, for example Ge, Ti, P, Fe, Ga, B and thus form zeolite analogues. Zeolites and their analogues are crystalline materials with regular microporous structure (with pore width < 2 nm). The intracrystalline pores are thus of molecular dimensions. The surface of intracrystalline pores is formed by oxygen atoms. The critical pore width is for atoms and molecules as a rule determined by oxygen rings containing 8, 10 or 12 oxygen atoms. Small cations can pass even through 6-membered oxygen rings. Micropores can accommodate spherical molecules typically with the diameter of 0.3-1.0 nm or cylindrical molecules with cylinder diameter in the above range. Zeolites are also called molecular sieves due to possible exclusion of molecules with size exceeding some critical value. Zeolites are perspective materials for industrial applications due to their molecular sieve effect, high adsorption capacity, and frequently to the presence of catalytic sites or to their ion exchange capability. A relatively novel zeolite SSZ-16 belongs to the class of small pore zeolites characterized by 8-membered oxygen rings which may exhibit molecular sieve effect for gases with small molecules. The main field of its application is believed to be in gas separation of various hydrocarbons and mixtures containing molecules such as CO_2, H_2, CH_2 and other gases [1–3]. Furthermore, zeolite SSZ-16 can be used as microporous layers and particles to develop composite and mixed matrix materials [4–6]. Zeolite SSZ-16 was also tested as a catalyst. For example, Cu-SSZ-16 [7, 8] seems to be promising as a selective catalytic reduction catalyst for the direct conversion of NO into N_2 and O_2. Zeolite H-SSZ-16 was found to be highly selective to dimethylamine in the catalytic reaction of ammonia and methanol [9]. The principal aim of this work is to optimize zeolite SSZ-16 hydrothermal synthesis and contribute to answering questions concerning limits to phase purity, yield and posibility to control morphology and size of crystals. Moreover, the research could clarify the role of diquaternary ammonium species in the synthesis. The principal aim of this work is to contribute to the knowledge of structure-directing agent (diquaternary ammonium dications) chemistry in relation to its (i) synthesis and purity, (ii) role in the synthesis of SSZ-16 zeolite, (iii) stability in synthesis batches and (iv) its thermal removal from the zeolite framework.

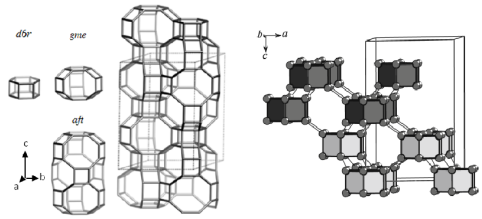

FIGURE 1. Left AFX framework type representation using CBU and their arrangement (adapted from www.iza-online.org), right - AFX framework type representation using 6-6 SBU (adapted from Ilyushin et al. 2015).

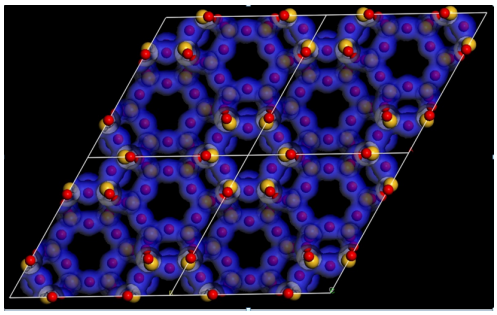

FIGURE 2. View of the AFX structure along the c-axis; yellow spheres - T-atoms, red spheres - oxygen atoms, blue patterns - visualization of electron density distribution.

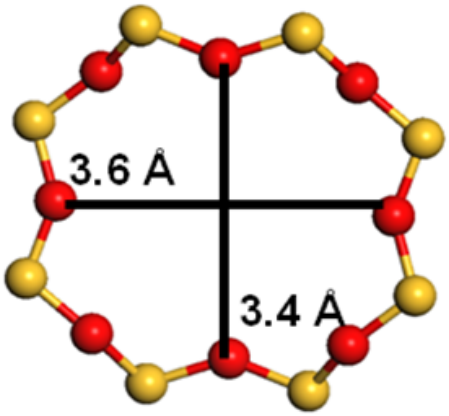

FIGURE 3. 8-membered oxygen ring in SAPO-56 viewed normal to [001], red spheres - oxygen atoms, yellow spheres - T-atoms

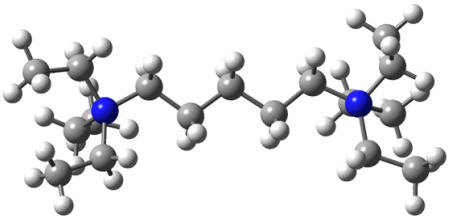

FIGURE 4. Structure of SDA - hexaethylpentane diammonium dication (blue spheres - nitrogen N^+, grey - carbon, white - hydrogen).

2. THEORY

2.1. ZEOLITE SSZ-16 AND ITS STRUCTURE

Zeolite SSZ-16 is isotypic with its zeolite analogue SAPO-56 [7, 10, 11]. Both these microporous materials exhibit the AFX framework type. This framework shows the hexagonal symmetry, the corresponding space group of symmetry is $P6_3/mmc$ and the unit cell idealized parameters are a = b = 13.7 Å, c = 19.7 Å. Fundamental articles on SSZ-16 present the AFX framework type in the terms of composite building units (CBU): gmelinite (gme) and aft cavities and d6r (double six-ring) cages [10, 12, 13], see Figure 1 (left). This method of AFX framework type representation is widely used to visualize spaces capable of accommodating sorbing species. However, this method is less suitable for the analysis of various zeolite framework topology features due to the existence of common T-atoms for the neighbouring CBU. An alternative way of AFX framework representation is by secondary building units (SBU) using either an array of 6-membered rings (6 code) or double 6-membered rings (6-6 code), see Figure 1 (right). Figure 2 represents the view of the AFX structure along the c-axis using the visualization of electron density distribution (computed by DFT calculation implemented in Castep program).

Zeolites SSZ-16 and SAPO-56 belong to small-pore zeolites with 3D pore system. The narrowest passages through these pores (also called bottlenecks or constrictions) are formed by 8-membered oxygen rings. Dimensions of these rings were published for SAPO-56 [11], see Figure 3.

2.2. ROLE OF SDA SPECIES IN SYNTHESIS OF SSZ-16

Essential components for zeolite synthesis are silica, alumina, source of alkali, SDA and water. Theoretical approaches offer a great number of hypothetical zeolite structures. However, only a small fraction of them can be synthesized. Besides, a considerable number of zeolite phases can be formed only in the presence of particular organic species termed as structure-directing agents (SDA). A mechanism of SDA action in synthesis mixtures is still an open question. Attempts were made to explain SDA effect on the basis of SDA species size and shape, its rigidity, hydrophobicity/hydrophilicity and SDA species interactions with solution components. Diquaternary ammonium species were proposed in the nineties as a novel group of SDA species for the synthesis of zeolites. The research in our laboratory showed that hexaethylpentane diammonium dication $(C_2H_5)_3N^+(CH_2)_5N^+(C_2H_5)_3$ (also called as Et_6-diquat-5^{2+}), appears to be, among diquaternary ammonium species, the most efficient SDA for the synthesis of zeolite SSZ-16 [14]. The model of this SDA dication is shown in Figure 4.

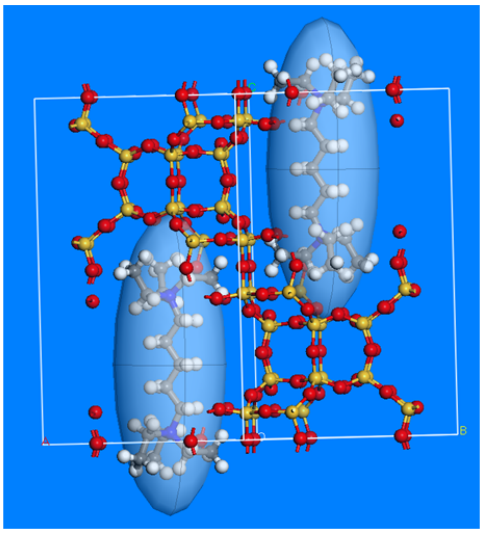

Figure 5. Computer simulated location of SDA molecules in UC of SSZ-16

A theoretical picture of SDA species in SSZ-16 structure was derived using the following assumptions:

- A non-decomposed SDA dication can be accommodated only in the aft cavity and thus oriented with its maximum dimension along the c-axis (see Figure 5).
- Any aft cavity accomodates just a single SDA dication.
- There are two aft cavities per UC. Therefore, the UC contains two SDA dications non-decomposed during the synthesis procedure.
- In principle, the gme cavities can accomodate only some products of SDA decomposition; this phenomenon is not considered in the theoretical estimate of SDA content.

Based on these assumptions, the following formula for SDA dication mass fraction $(g_{SDA})^{th}$ in molar mass of UC for non-calcined zeolite SSZ-16 can be formulated as

$$(g_{SDA})^{th} = \frac{N_{SDA}\ \ M_{SDA}}{(M_{UC})_0 + N_{SDA}\ \ M_{SDA}},$$

where N_{SDA} stands for the number of SDA per UC and is equal to 2, M_{SDA} denotes the molar mass of SDA and equals to $272.32\,\mathrm{g\,mol^{-1}}$. $(M_{UC})_0$ represents the molar mass of zeolite SSZ-16 free of SDA and can be expressed depending on the atomic ratio Si/Al = z as

$$(M_{UC})_0 = \frac{48\ M_{Na}}{1+z} + \frac{48\ M_{Si}\ z}{1+z} + \frac{48\ M_{Al}}{1+z} + 96\ M_O,$$

for z = 6 and $(M_{UC})_0 = 3029.23\,\mathrm{g\,mol^{-1}}$.

Based on these equations, the SDA dication mass fraction $(g_{SDA})^{th}$ can be calculated and it equals to 0.152. The experimentally measured SDA content $(g_{SDA})^{th}$ in the zeolite synthesis product will be compared to this value.

3. Experimental

3.1. Synthesis of SDA

In view of the fact that the price of species containing Et_6-diquat-5^{2+} dication appeared to be prohibitive, a protocol for its synthesis was developed. The reactants used for this purpose were 1,5-dibromopentane and triethylamine. The reaction proceeded in ethanol solvent. The crystallization was performed in diethyl ether solvent. Because the synthesis proceeds in two-stages, the purity of the synthesis product were examined by X-ray diffraction and by thermogravimetry. The heating program for SDA thermogravimetry was the same as for zeolite samples calcination and zeolite thermogravimetry, see below. SDA with significant content of the first stage synthesis product can thus be rejected or recycled.

3.2. Synthesis of SSZ-16 particles

The research was directed to the development of a static in-situ hydrothermal crystallization procedure of SSZ-16 zeolite [14, 15]. The synthesis was performed in three steps: Preparation of starting synthesis mixture, ageing of synthesis mixture (formation of viable nuclei), and crystallization of aged mixture. The most suitable silica source appeared to be colloidal silica. The starting synthesis mixture was composed of colloidal silica LUDOX AS 30 (30% Sigma-Aldrich), aluminum nitrate nonahydrate, sodium hydroxide, organic template Et_6-diquat-5 Br_2 and deionized water [14, 16]. The synthesis process was adapted by changing the synthesis solution composition, ageing period, temperature and duration of crystallization [15, 16]. The composition of synthesis solution was varied and optimized to obtain pure phase of SSZ-16 particles. The ageing period was performed for seven days to promote nucleation of precursor particles (formation of viable nuclei). The ageing process of SSZ-16 was performed at elevated temperature with the synthesis solutions heated up to 80 °C inside an oil bath, continuous stirring was ensured by a magnetic stirrer inside Teflon vessels. The crystallization process was performed for seven days, temperature adjusted to 160 °C. The hydrothermal in-situ synthesis of SSZ-16 crystalline particles performed inside Teflon-lined stainless steel stationary autoclaves from the pre-aged solutions under autogenous pressure. The crystalline SSZ-16 products were purified inside an ultrasonic bath, washed and dried in a pre-heated oven overnight. After the synthesis, the SDA was removed by the two-cycle thermal calcination process under nitrogen/air atmosphere to open pores inside the aft cage. The temperature program for both the cycles was as follows: heating with the rate 0.5 °C/min to 120 °C, keeping at 120 °C for two hours, heating to the temperature 550 °C with the rate 0.5 °C/min, then keeping at 550 °C for 8 hours and cooling to the room temperature with the rate 0.5 °C/min.

3.3. Characterization

Zeolite SSZ-16 particles were characterized by Scanning Electron Microscopy (SEM) technique using JEOL JSM 5500LV to examine crystal morphology and particle size. Powder X-ray diffraction (XRD) technique was used to determine crystallinity and phase purity of zeolite SSZ-16 particles. X-ray diffraction was performed on PANalytical X'Pert PRO diffractometer with Co anode (wavelength $\lambda = 0.1789$ nm) in Bragg-Brentano geometry. The fixed divergent slits in primary beam and 1D detector X'Celerator in diffracted beam were used. The spectra were collected in the 2θ range of 5-30°. The measurements and analyses of collected spectra were performed in the Institute of Physics, CAS. The micropore volume of calcined zeolite SSZ-16 particles was evaluated from nitrogen adsorption-desorption isotherms. The isotherms were measured on ASAP 2020 (Micromeritics, USA) volumetric instrument at -196 °C. The sample was degassed under a vacuum at 350 °C for 8 h prior to the analysis. The micropore volume was evaluated by the t-plot method. Particular attention was paid to SDA. It concerned SDA purity (XRD analysis), thermal stability and its decomposition both in synthesis solutions and products. Thermal stability of SDA in alkaline solutions were analyzed after the heat treatment in an autoclave. SDA concentration was measured using cyclic voltammetry (CV) [17] with the home-made apparatus in J. Heyrovsky Institute of Physical Chemistry, CAS. SDA content in zeolite samples and SDA residua after their calcination were measured using elemental analysis performed on Elementar Vario EL III in CHNS operation mode, and further on with X-ray Photoelectron spectroscopy XPS using ESCA 3 Mk II spectrometer (VG) in fixed transmission mode. The kinetics of SDA removal/decomposition and related heat effects were investigated with thermogravimetry and differential scanning calorimetry using SetSys Evolution TGA, Setaram.

4. Results and Discussion

Among silica sources for synthesis mixtures, LUDOX-based synthesis mixtures had the best properties both from the point of view of hydrogel density and capacity of crystallization. Optimum synthesis batch composition to eliminate unwanted phases in product was determined as 3 SDA: 15 Na_2O: 0.5 Al_2O_3: 30 SiO_2: 1200 H_2O. Deviation from this composition causes considerable changes in phase composition and formation of different zeolitic phases. The introduction of LUDOX AS 30 as silica source had two consequences: (i) reducing the size of amorphous core of zeolite particles which was observed in the early stages of synthesis procedure development (see Figure 6A) and (ii) dramatic reducing the size of particles. The size of particles decreased to approximately 2 µm and well-developed polycrystalline particles formed (see Figure 6B). This favourable development of product quality manifests itself also (i) in X-ray spectra (see

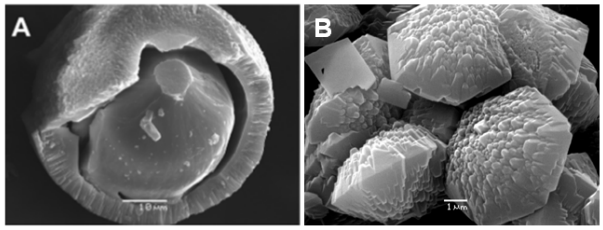

Figure 6. A - amorphous core and crystalline shell of a particle (2 000×), B - well developed polycrystalline particles (10 000×).

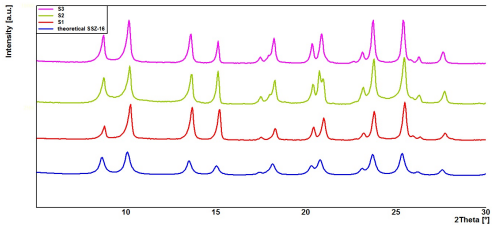

Figure 7. XRD spectra of selected samples and theoretical spectrum of SSZ-16

Figure 7) and (ii) in SDA content measured gravimetrically from mass difference between non-calcined and calcined samples, showing on selected zeolite samples the development of $(g_{SDA})^{exp}$. In contrast to earlier preparations where amorphous cores were visible on disrupted particles and the values of $(g_{SDA})^{exp}$ ranged between 0.160 and 0.180, in more recent experiments the amorphous cores were not observed and $(g_{SDA})^{exp}$ ranged between between 0.140 and 0.150 approximately. It is suspected that amorphous cores exhibited a higher content of SDA as compared with zeolite phase.

Figure 7 represents an example of the X-ray diffraction spectra of selected calcined samples compared to the theoretical diffraction spectrum for the zeolite SSZ-16. The samples were confirmed to be crystalline and pure phase SSZ-16 particles.

Regarding the content of organic species in the synthesized zeolite, a question arises whether some decomposition products of SDA cannot be located in gme cavities. The evaluation of SDA thermal stability in alkaline solutions performed by cyclic voltammetry showed a relatively rapid SDA decomposition. The time dependence of SDA concetration during its thermal treatment in alkaline solution at temperature, pH, and SDA concentration close to those in synthesis mixtures is shown in Figure 8. It is obvious that during the reaction time 6 to 8 hours the SDA concentration decreases to a value lower than 50 % of its initial value. This may generate a considerable number of SDA fragments and enhance the mass of organics incorporated in SSZ-16 crystals. Nevertheless, for optimized synthesis procedure the values of $(g_{SDA})^{exp}$ remain in the range 0.140 to 0.150 which cast doubt on additional places of organics accommodation in SSZ-16 crystals.

Accessibility of microporous crystal cavities after

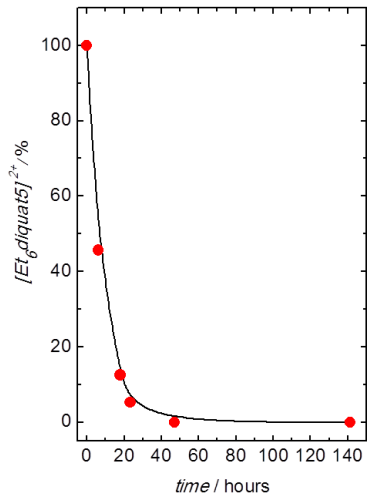

Figure 8. Kinetics of Et_6-diquat-5^{2+} decomposition at 160 °C. Initial concentration of Et_6- diquat-5 Br_2 $c^0{}_{SDA} = 0.168\,\mathrm{mol\ dm^{-3}}$, initial concentration of NaOH $c^0{}_{SDA} = 1.66\,\mathrm{mol\ dm^{-3}}$, solvent deionized water.

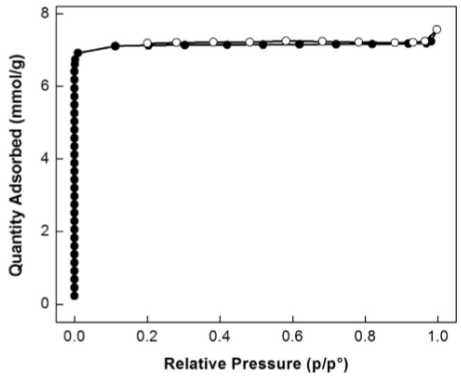

Figure 9. N_2 adsorption-desorption isotherm. Full circles - adsorption, empty circles - desorption.

template removal was confirmed by measurements of adsorption and desorption isotherms of N_2 at -196 °C. This result is exemplified by isotherms measured on calcined sample (Figure 9). The isotherm shows a sharp rise in N_2 adsorption at low relative pressure and negligible hysteresis loop. Its shape shows that the material is microporous with negligible effect of mesopores. The sample showed the micropore volume of 0.24 $\mathrm{cm^3\,g^{-1}}$. At the same time, the elemental analysis excluded presence of organic residua in crystal bulk after SSZ-16 calcination. This is a contrast to the situation in crystal subsurface region where carbonaceous deposits were detected after zeolite calcination by XPS.

The thermogravimetric curves monitored during SDA removal from zeolite samples using the above temperature program are exemplified on Figure 10. Temperature calibration was performed using $CuSO_4.5H_2O$ and Sn. On the picture is the comparison of SDA removal from silicalite-1 (TPA^+) with that from SSZ-16 (Et_6-diquat-5^{2+}). There is bigger amount of organics in SSZ-16 and steeper decay in the first portion of the TG curve. We suspect that it may be related to more rapid thermal decomposition of Et_6-diquat-5^{2+} in synthesis batch as compared with TPA^+ in silicalite-1 which is considerably more stable. We also suspect that SDA fragments may be incorporated into gme cavities.

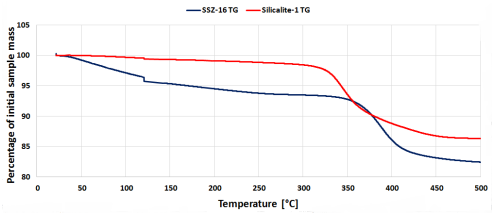

Figure 10. Examples of TG curves - percentage of the sample mass based on initial mass vs. temperature; red - silicalite-1 templated with TPA^+; blue - SSZ-16 templated with Et_6-diquat-5^{2+}.

5. Conclusions

The principal contribution of this work is the feasibility of zeolite SSZ-16 synthesis. The selected SDA hexaethylpentane diammonium cation turned out to be appropriate and the synthesis route to this species was elaborated. By variation of synthesis parameters of aging and crystallization, the particle size was reduced from cca 50 µm to approximately 2 µm. Moreover, the conditions to attain purity of SSZ-16 higher than 98 % were found and polycrystalline samples with well developed morphology were obtained. Using N_2 adsorption and desorption at -196 °C, volume of micropores $V_{micro} = 0.24\ \mathrm{cm^3\,g^{-1}}$ was evaluated. An insight into the chemistry of SDA was presented. In particular, in its synthesis and conditions of its purity. Further on, a novel technique was introduced to measure concentration variation of cationic SDAs under conditions close to those at synthesis conditions. Particular attention was also paid to the investigation of template removal kinetics.

Acknowledgements

The financial support by Czech Science Foundation via grant GA16-02681S is gratefully acknowledged.

References

[1] M. Pera-Titus et al. Porous inorganic membranes for co2 capture: Present and prospects. *Chem Rev* **114**(2):1413–1492, 2014. doi:10.1021/cr400237k.

[2] J. Caro et al. Zeolite membranes - recent developments and progress. *Microporous Mesoporous Mater* **15**(3):215–233, 2008. doi:10.1016/j.micromeso.2008.03.008.

[3] S. G. Li et al. Improved sapo-34 membranes for co2/ch4 separations. *Adv Mater* **18**(19):2601–2603, 2006. doi:10.1002/adma.200601147.

[4] M. Moliner et al. Synthesis strategies for preparing useful small pore zeolites and zeotypes for gas separations and catalysis. *Chem Mater* **26**(1):246–258, 2014. DOI:10.1021/cm4015095.

[5] R. Krishna et al. Separating n-alkane mixtures by exploiting differences in the adsorption capacity within cages of cha, afx and eri zeolites. *Sep Purif Tech* **60**(3):315–320, 2008. DOI:10.1016/j.seppur.2007.09.008.

[6] N. Kosinov et al. High flux high-silica ssz-13 membrane for co2 separation. *J Mater Chem A* **2**(32):13083–13092, 2014. DOI:10.1039/c4ta02744b.

[7] D. W. Fickel et al. The ammonia selective catalytic reduction activity of copper-exchanged small-pore zeolites. *Appl Catal B* **102**(3-4):441–448, 2011. DOI:10.1016/j.apcatb.2010.12.022.

[8] M. J. Wulfers et al. Conversion of methane to methanol on copper-containing small-pore zeolites and zeotypes. *Chem Comm* **51**(21):4447–4450, 2015. DOI:10.1039/C4CC09645B.

[9] H. Y. Jeon et al. Catalytic evaluation of small-pore molecular sieves with different framework topologies for the synthesis of methylamines. *Appl Catal A* **305**(1):70–78, 2006. DOI:10.1016/j.apcata.2006.02.044.

[10] R. F. Lobo et al. Synthesis and rietveld refinement of the small-pore zeolite ssz-16. *Chem Mater* **8**(10):2409–2411, 1996. DOI:10.1021/cm960289c.

[11] S. T. Wilson et al. Synthesis, characterization and structure of sapo-56, a member of the abc double-six-ring family of materials with stacking sequence aabbccbb. *Microporous Mesoporous Mater* **28**(1):125–137, 1999. DOI:10.1016/S1387-1811(98)00293-5.

[12] Y. Bhawe et al. Effect of cage size on the selective conversion of methanol to light olefins. *ACS Catal* **2**(12):2490–2495, 2012. DOI:10.1021/cs300558x.

[13] P. Y. Feng et al. Synthesis and single crystal structure of an afx-type magnesium aluminophosphate. *Microporous Mesoporous Mater* **50**(2-3):145–149, 2001. DOI:10.1016/S1387-1811(01)00441-3.

[14] S. H. Lee et al. Zeolite synthesis in the presence of flexible diquaternary alkylammonium ions (c(2)h(5))(3)n(+)(ch(2))(n)n(+)(c(2)h(5))(3) with n=3-10 as structure-directing agents. *Microporous Mesoporous Mater* **60**(1-3):237–249, 2003. DOI:10.1016/S1387-1811(03)00381-0.

[15] P. Hrabanek et al. Static in-situ hydrothermal synthesis of small pore zeolite ssz-16 (afx) using heated and pre-aged synthesis mixtures. *Microporous Mesoporous Mater* **228**:107–115, 2016. DOI:10.1016/j.micromeso.2016.03.033.

[16] P. Hrabanek et al. Combined silica sources to prepare preferentially oriented silicalite-1 layers on various supports. *Microporous Mesoporous Mater* **174**(1-3):154–162, 2013. DOI:10.1016/j.micromeso.2013.03.007.

[17] J. Langmaier et al. Extreme basicity of biguanide drugs in aqueous solutions: Ion transfer voltammetry and dft calculations. *J Phys Chem A* **120**:7334–7350, 2016. DOI:10.1021/acs.jpca.6b04786.